

Visualization and analysis of EPS glycoconjugates of the thermoacidophilic archaeon *Sulfolobus metallicus*

Ruiyong Zhang¹ · Thomas R. Neu² · Yutong Zhang¹ · Sören Bellenberg¹ · Ute Kuhlicke² · Qian Li¹ · Wolfgang Sand¹ · Mario Vera¹

Received: 9 March 2015 / Revised: 14 June 2015 / Accepted: 17 June 2015 / Published online: 14 July 2015
© Springer-Verlag Berlin Heidelberg 2015

Abstract Biofilms are surface-associated colonies of microorganisms embedded in a matrix of extracellular polymeric substances (EPS). As EPS mediate the contact between cells and surfaces, an understanding of their composition and production is of particular interest. In this study, the EPS components of *Sulfolobus metallicus* DSM 6482^T forming biofilms on elemental sulfur (S⁰) were investigated by confocal laser scanning microscopy (CLSM). In order to visualize cell and EPS distributions, biofilm cells were stained with various dyes specific for glycoconjugates, proteins, nucleic acids and lipids. Biofilm cells on S⁰ were heterogeneously distributed and characterized as individual cells, microcolonies, and large clusters up to a hundred micrometers in diameter. The glycoconjugates in biofilms were detected by fluorescence lectin-binding analysis (FLBA). Screening of 72 commercially available lectins resulted in the selection of 21 lectins useful for staining biofilms of *S. metallicus*^T. Capsular EPS from planktonic cells were mainly composed of carbohydrates and proteins. In contrast, colloidal EPS from planktonic cells were dominated by carbohydrates. Proteins were found to be major components in EPS from biofilms on S⁰. Using specific probes combined with CLSM, we showed that extracellular proteins and nucleic acids were present in the EPS matrix.

Finally, we showed that *S. metallicus*^T cells were embedded in a flexible EPS matrix. This study provides new insights into archaeal biofilms and EPS composition and properties with respect to their interactions with S⁰.

Keywords Biofilm · Glycoconjugates · Thermoacidophilic archaea · Lectin · Elemental sulfur

Introduction

Sulfur is important in central biochemistry as well as in industrial applications such as sulfur concretes, sulfur foams, sulfur asphalts, and sulfuric acid production. The biological sulfur cycle has important environmental and economic significance for many fields such as acid mine drainage (AMD), soil acidification, and material corrosion (Little et al. 2000). Sulfur-metabolizing acidophilic bacteria and archaea oxidize various reduced inorganic sulfur compounds (RISCs) that occur naturally (Dopson and Johnson 2012). Protons generated from microbial sulfur oxidation are an important agent to accelerate and cause dissolution of metal sulfides. In addition, the resulting acidic environments are essential for metal-oxidizing microorganisms to thrive. From another point of view, as one of the major intermediates in the course of metal sulfide oxidation (Sand et al. 1998), S⁰ and polysulfides may form a passive layer during chalcopyrite (CuFeS₂, a refractory copper mineral) dissolution and, subsequently, metal leaching is hindered (Dutrizac 1990; Rodriguez et al. 2003).

The microbial biofilm lifestyle brings various advantages such as mechanical stability, nutrient supply, and genetic exchange as well as protection from dehydration and environmental stress (Flemming and Wingender 2010). EPS include carbohydrates, proteins, lipids, and DNA among other macromolecules (Flemming et al. 2007). To date, studies on microbial

Electronic supplementary material The online version of this article (doi:10.1007/s00253-015-6775-y) contains supplementary material, which is available to authorized users.

✉ Mario Vera
mario.vera@uni-due.de

¹ Aquatische Biotechnologie, Biofilm Centre, Universität Duisburg—Essen, Universitätsstraße 5, 45141 Essen, Germany

² Department of River Ecology, Helmholtz Centre for Environmental Research—UFZ, Brückstraße 3a, 39114 Magdeburg, Germany

biofilms and EPS have mainly been conducted on bacteria. In contrast, only very limited information is available for the archaeal domain, in which biofilms are as widespread and complex as the bacterial ones (Fröls 2013; Orell et al. 2013).

Attachment of microbes to sulfur is dependent on growth conditions, hydrophobic interactions, and other factors like osmotic pressure (Knickerbocker et al. 2000; Takeuchi and Suzuki 1997). Surfactants (e.g., Tween 80) were shown to be stimulatory for microbial growth and sulfur oxidation by *Acidithiobacillus albertensis* and *Acidithiobacillus ferrooxidans* (Sand 1985; Zhang et al. 2008a). Extracellular lipids (e.g., phospholipids), acting as a wetting agent, can also mediate microbial interactions with sulfur and are thought to play key roles during its oxidation (Arredondo et al. 1994). Also, microbial appendages (filamentous matrix) or extracellular compounds (glycocalyx) were found to play a role in sulfur colonization and oxidation by *Acidithiobacillus thiooxidans* and *A. albertis* (Blais et al. 1994; Bryant et al. 1984). These studies also indicate that microbial attachment may be a consequence of different mechanisms, e.g., attachment of *A. thiooxidans* and *A. albertis* to sulfur surface was favored by the presence of filamentous materials to a bacterial glycocalyx. However, sulfur colonization by *Thiobacillus thioparus* did not follow this attachment mechanism (Blais et al. 1994).

Sulfur oxidation by acidophilic microbes may involve the following steps: (1) cell attachment to and colonization of sulfur surfaces by chemotaxis and hydrophobic interactions among others; (2) a S^0 activation prior to oxidation (Rohwerder and Sand 2003), possibly conducted by thiol-rich proteins excreted after cell colonization (Peng et al. 2013; Zhang et al. 2008b); (3) a (yet unclear) process of transport of sulfur and/or polysulfides through the cell membrane; and (4) oxidation of sulfur in the periplasmic space (in case of Gram-negative bacteria) or cytoplasm, where sulfur oxidizing enzymes (e.g., the archaeal sulfur oxygenase-reductase, SOR) are located. Although RISC speciation during sulfur and mineral sulfide oxidation by *Sulfobacillus thermosulfidooxidans* and *Acidianus manzaensis* has been recently described (Liu et al. 2013; Nie et al. 2014), transformation of various sulfur allotropes makes the understanding of sulfur metabolism difficult. Current understanding of sulfur chemolithotrophic oxidation in Archaea is largely restricted to *Sulfolobales*, e.g., *Sulfolobus* and *Acidianus* (Kletzin 2008; Rohwerder and Sand 2007).

The archaeal cell envelope and surface structures are fundamentally different from the bacterial ones (Albers and Meyer 2011). Archaea and bacteria may use different surface compounds and mechanisms to interact with their surrounding environment. Most previous biofilm studies were mainly done using (preparative) destructive approaches, e.g., scanning electron microscopy (SEM) or transmission electron microscopy (TEM). In contrast, fluorescence lectin-binding analysis (FLBA) and attenuated total reflection-Fourier transform infrared (ATR-FTIR) spectroscopy are both non-destructive techniques for analyzing

biofilm formation and EPS components (Schmitt and Flemming 1998; Zippel and Neu 2011). FLBA usually involves screening of many lectins to establish a panel of probes which react with a particular biofilm sample and which may indicate the composition of EPS glycoconjugates in biofilms. The first FLBA of acidophilic archaeal biofilms revealed that various glycoconjugates, e.g., glucose, galactose, mannose, N-acetylglucosamine (GlcNAc), N-acetylgalactosamine (GalNAc), sialic acids, and fucose, were present in biofilms of *Ferroplasma acidiphilum*, *Sulfolobus metallicus*, and *Acidianus* sp. DSM 29099 grown on pyrite (Zhang et al. 2015). Fourier transform infrared (FTIR) is widely used to analyze functional groups in mixed biofilms and also to identify microbes at the strain level according to specific surface infrared spectra. In addition, key band ratios within a defined spectrum of a biological sample can correlate with the composition of biological materials and provide useful information about environmental biofilm samples (Nichols et al. 1985).

The Crenarchaeon *S. metallicus* is a thermoacidophilic obligate aerobe with an optimal growth temperature at 65 °C and an optimal growth pH of 2–3. It oxidizes ferrous iron, RISCs (e.g., S^0 , tetrathionate), and metal sulfides. *S. metallicus* is the only species of this genus which can grow chemolithotrophically using metal sulfides or RISCs to sustain growth. In addition, compared to the mesophilic and moderate thermophilic archaeal and bacterial counterparts, *S. metallicus* grows at higher temperatures, leading to increased metal sulfide leaching rates.

In this report, biofilm formation and EPS matrix components were studied based on an in situ and non-destructive approaches using ATR-FTIR and FLBA. *S. metallicus* DSM 6482^T was used as the model organism for screening 72 commercially available fluorescent-labeled lectins. These lectins which react with EPS glycoconjugates of *S. metallicus*^T were obtained for in situ monitoring of biofilm development and potentially probing individual species in mixed biofilms. In addition, different EPS compounds including nucleic acids, proteins, and lipophilic compounds as well as various glycoconjugates were visualized by confocal laser scanning microscopy (CLSM). FTIR was used to identify functional groups (biopolymers) likely to be involved in microbial attachment to and biofilm formation on S^0 . Conventional spectrophotometric methods were used to determine EPS components from planktonic and biofilm cells. This is the first report of biofilm and EPS analysis of *S. metallicus* grown on S^0 .

Experimental procedures

Archaeal strains and growth conditions

S. metallicus DSM 6482^T was purchased from Deutsche Sammlung von Mikroorganismen und Zellkulturen GmbH

(DSMZ). The new isolate *Acidianus* sp. DSM 29099 (=JCM 30227) was chosen to study the biofilm features and EPS production comparatively with *S. metallicus*^T. Both strains were grown in Mackintosh (MAC) medium (Mackintosh 1978) at 65 °C and 120 rpm with an initial pH of 2.5. S⁰ (10 g/L) and yeast extract (0.2 g/L) were added as energy source and growth factors, respectively.

Sulfur prills and cubes

To produce sulfur prills and cubes, sulfur powder (Carl Roth, Germany) was molten in a glass beaker at 130 °C and poured into ice-cold deionized water with agitation (250 rpm). Sulfur prills with a diameter of 1–3 mm were formed due to rapid cooling. Also, molten sulfur was poured on glass plates to obtain a sulfur layer after its solidification. Sulfur coupons with a size of approx. 0.5 cm × 0.5 cm × 2 mm were obtained by breaking the sulfur layer. Both, sulfur prills and coupons, were autoclaved at 110 °C for 90 min.

EPS extraction and analysis

After 7 days of incubation, planktonic cells and sulfur particles with biofilm cells were separated by filtration through sterile Whatman filter paper. Cells of *S. metallicus*^T were collected afterwards by centrifugation at 8000 rpm (11,300 g) for 15 min. Cell pellets were washed by MAC medium and freeze-dried (ALPHA 2–4 LSC, –80 °C). The supernatant was further filtrated through polycarbonate filters (GTTB, Ø2.5 cm, 0.2 µm pore size, Millipore®) to remove whole cells. These cell-free supernatants (containing “colloidal EPS”) were dialyzed using a cellulose membrane (cutoff 3.5 kDa) against deionized water at 4 °C for 48 h. Dialyzed colloidal EPS solutions were further freeze-dried. Capsular EPS were extracted from cell pellets using 20 mM EDTA as previously described (Castro et al. 2014). Sulfur particles were manually milled in a mortar and incubated with 20 mM EDTA at 4 °C and shaking at 180 rpm for 4 h to extract EPS from biofilm cells. The extraction was repeated three times and the resulting solutions were centrifuged, filtered, and dialyzed as described above.

Phenol–sulfuric acid method was used for carbohydrate determination with glucose as a standard (Dubois et al. 1956). Protein concentration was analyzed with bovine serum albumin (BSA) standard (Bradford 1976). DNA was determined using DNA from salmon sperm as a standard (Burton 1956). Cell lysis was estimated by measuring glucose-6-phosphate dehydrogenase activity (Ng and Dawes 1973).

Fourier transformed infrared spectroscopic assay

Powdered cell pellets, colloidal EPS, and EPS extracted from *S. metallicus*^T biofilms on S⁰ were spread on a diamond attenuated total reflectance (ATR) apparatus (Pike Technologies,

USA), separately attached to the FTIR. The spectra were recorded using a FTIR 430 spectrometer (JASCO, Japan). The baseline shift of blank spectra was corrected using Spectra Manager (JASCO, Japan). At least 64 scans, with a resolution of 4 cm⁻¹, were collected for all samples using the Happ-Genzel apodization function. Two measurements were done for each sample. As all cellular components possess characteristic absorbance frequencies and primary molecular vibrations between 4000 and 550 wave numbers (Naumann et al. 1991), the FTIR scan was carried out in this region.

Fluorescence staining of samples

Sulfur prills and coupons with attached cells were mounted in a Petri dish. The cell biomass and spatial distribution within the biofilms on S⁰ were visualized after staining with the nucleic acid stains: DAPI (diamidino-2-phenylindole), Syto 9, Syto 61, Syto 64, SybrGreen (Invitrogen, Germany), and DDAO (7-hydroxy-9H⁻¹,3-dichloro-9,9-dimethylacridin-2-one; Invitrogen, Germany). The cell-permeant Syto 64, a fluorescent nucleic acid stain, exhibits bright red fluorescence upon binding to nucleic acids. DDAO stains nucleic acids and normally does not penetrate cell membranes. Thus, it has been selected as the preferred fluorochrome for staining extracellular DNA (eDNA) (Koerdet et al. 2010). DDAO was incubated with samples for 20 min before CLSM observation. All other dyes were added to the samples and directly visualized. In addition, stains specific for proteins, lipophilic compounds, and β-polysaccharides were also tested to characterize biofilm components. The details of these stains are listed in Table 1.

Fluorescence lectin-binding assays

Based on a critical assessment of the lectin approach for EPS glycoconjugates (Neu et al. 2001), mainly FITC-labeled lectins but also some Alexa-labeled lectins were tested to select suitable ones for binding to *S. metallicus* biofilms. Staining was done in a Petri dish or a coverwell chamber of 20 mm in diameter with 0.5 mm spacer (Invitrogen, Germany) as described before (Zhang et al. 2015). In case of counter staining, lectin-stained samples were incubated with nucleic acid/protein/lipid stains and directly observed using CLSM without any further treatment. For staining cells from the planktonic phase, 1 mL of cultures grown for 4 days were filtered on polycarbonate filters as previously described (Bellenberg et al. 2012) and incubated with 16 selected lectins (Supplementary Table S1). Filters with stained cells were mounted using an anti-fading agent (Citifluor, Ltd. AF2) prior to CLSM observation.

Confocal laser scanning microscopy

Examination of stained samples was performed using a TCS SP5X AOBS (Leica, Heidelberg, Germany), controlled by the

Table 1 Characteristics and binding targets of selected fluorochromes used in this study

Fluorochrome	Binding targets	Ex/Em wavelength (nm)	Concentration
SYTO 9	Nucleic acids (NA)	483/478–488, 500–560	6 μM
SYTO 64	NA	599/625–700	6 μM
SybrGreen	NA	483/475–489, 500–560	6 μM
DDAO	Extracellular NA	600/620–720	10 $\mu\text{g/mL}$
DAPI	NA	405/485–495, 515–600	100 $\mu\text{g/mL}$
SyproRed	Proteins	475, 500/470–480, 580–680	$\times 1$ work solution
SyproOrange	Proteins	475/470–480, 520–620	$\times 1$ work solution
FMI-43	Lipid-rich domain	475–485/580–650	10 $\mu\text{g/mL}$
FITC-conjugated lectins	EPS glycoconjugates	490/485–495, 510–600	50–100 $\mu\text{g/mL}$
Calcofluor white M2R	β -Polysaccharides	365/420–460	100 $\mu\text{g/mL}$
Nile red	Lipid-rich domain	550/650	10 $\mu\text{g/mL}$

All fluorochromes were from Invitrogen, except Nile red (Sigma Aldrich).

LASAF 2.4.1 build 6384. The system was equipped with an upright microscope and a super continuum light source (470–670 nm) as well as a 405-nm pulsed laser diode. Images were collected with a $\times 63$ water immersion lens with a numerical aperture (NA) of 1.2 and a $\times 63$ water immersible lens with a NA of 0.9. Details of fluorescent dyes along with excitation and emission filters used are shown in Table 1. CLSM data sets were recorded in sequential mode to avoid cross talk of the fluorochromes between two different channels. Surface topography and texture of the pyrite as well as of the S^0 surface were recorded by using the CLSM in reflection mode.

Atomic force microscopy and epifluorescence microscopy

A NanoWizard II atomic force microscope (JPK Instruments, Germany) combined with the BioMaterial Workstation (JPK Instruments) was used. For atomic force microscopy (AFM) imaging, a silicon cantilever CSC37-A (Mikromasch, Estonia) with the following features was used: typical length, 250 μm ; width, 35 μm ; thickness, 2 μm ; resonance frequency, 41 kHz; and nominal force/spring constant, 0.65 N/m. Each AFM image consists of 512 by 512 or 1024 by 1024 pixels. AFM imaging was performed in contact mode in air. Twenty microliters of cell suspension were spread on a glass slide and cells were fixed by evaporation. Cells and their EPS were stained by Syto 9 and TRITC-labeled Con A, respectively, as mentioned above. By using a shuttle stage, the same surface area of samples was both visualized by epifluorescence microscopy (EFM) (Zeiss, Germany) and AFM (BioMaterial™ Workstation, JPK Instruments) with an error below 2 μm (Mangold et al. 2008). At least three different spots (around 100 by 100 μm) from each sample were checked and recorded by combined AFM and EFM.

Digital image analysis

Fluorescence images were analyzed using an extended version of the software ImageJ. Maximum intensity (MIP) and XYZ projections of 3-dimensional data sets were produced with the software IMARIS version 7.3.1 (Bitplane AG, Zurich, Switzerland) and Huygens-Adobe. In some cases, deconvolution of 3-dimensional data sets was processed to enhance the clarity of the images.

Results

EPS characterization

The presence of functional groups on archaeal cells and S^0 surfaces was examined using FTIR spectroscopy. ATR-FTIR spectra of cells and EPS from biofilms as well as from colloidal EPS from supernatant of *S. metallicus*^T cultures are shown in Fig. 1. The spectra displayed different features which originate from various biopolymers. According to previous reports (Schmitt and Flemming 1998; Suci et al. 1997), the bands at approx. 1634 and 1536 cm^{-1} are due to proteins (amide I and amide II). Features with peaks at 1453 cm^{-1} are due to C-H bend from CH_2 . The band at 1389 cm^{-1} represents the C-O bend from carboxylate groups. Features with peaks at 1211 primarily originate from phosphodiester linkages of RNA and DNA. Polysaccharides normally exhibit bands in the region from 1130 to 900 cm^{-1} . Obviously, cells of *S. metallicus*^T have mainly proteins and carbohydrates on their surfaces, which is in agreement with the characteristics of *Sulfolobales*. By comparison of cells and EPS from biofilms, changes in the peak location and intensity of the amide groups were detected. This implies protein conformational variation (Parikh and Chorover 2006). In addition, EPS from biofilms showed small peaks in the polysaccharide region if compared

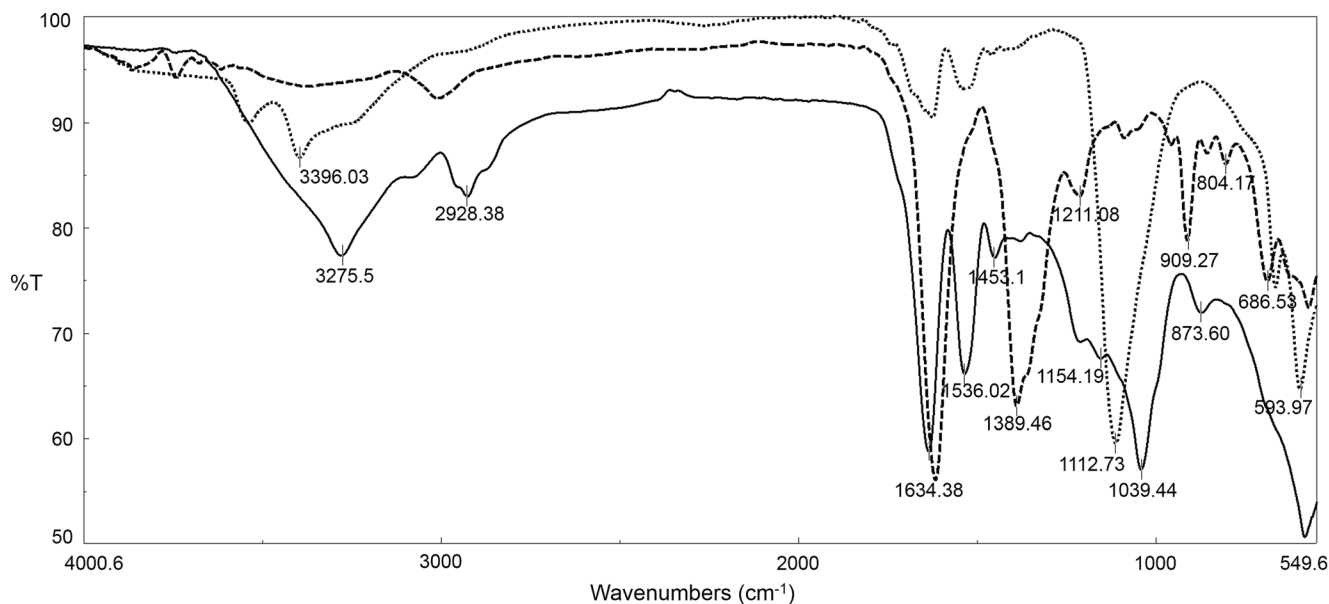


Fig. 1 ATR-FTIR spectra of cells and EPS of *S. metallicus*^T grown on S^0 . Planktonic cells (solid line), colloidal EPS (dotted line), and EPS from biofilms on S^0 (dashed line) are shown

to cell signals. The band ratios of amide I/polysaccharide from cell surface (~ 1) and EPS from biofilms (~ 2) were observed to change. This finding suggests an increased protein proportion in cells attached to S^0 . Colloidal EPS showed only a strong polysaccharide peak at 1039 cm^{-1} . The variation of the peak position of cells and colloidal EPS in the polysaccharide region indicates a variation of sugar moieties. ATR-FTIR spectra of S^0 collected after cell growth showed characteristics of the presence of biopolymers (e.g., amide I and II adsorption; not shown). By conventional spectrophotometric methods, both colloidal EPS and capsular EPS from planktonic cells were found to be composed of carbohydrates and proteins (Supplementary Table S2). In colloidal EPS, the amount of carbohydrates (25.9 mg/L) was ~ 9 times higher than proteins (2.9 mg/L). In contrast, similar amount of carbohydrates (15.9 mg/g) and proteins (15.7 mg/g) were found in capsular EPS fractions. In the case of EPS from biofilms on S^0 , proteins were the main components (8.8 mg/g). Also, carbohydrates (0.5 mg/g) and DNA (0.09 mg/g) were detected. In general, the spectrophotometric determination agreed with ATR-FTIR analysis. Taken together, EPS data indicated the following: (1) *S. metallicus*^T cells attached to S^0 were capable of modifying their surface, (2) protein-like compounds dominated on the S^0 surface, and (3) the compounds excreted to the bulk solution were mostly carbohydrates.

Visualization of planktonic cells of *S. metallicus*^T grown on S^0

Planktonic cells on glass slides Cells of *S. metallicus*^T appear as irregular shaped with a diameter of 1–1.5 μm when grown

on S^0 (Fig. 2b, c). In addition, by EFM, we observed that Syto 9 signals were mostly surrounded by Con A signals. This indicates that cells were covered with glycoconjugates rich in mannose and/or glucose. Obviously, the contact between cells and glass surfaces is mediated by these compounds. Few spots (footprints) were detected with only EPS signals devoid of nucleic acid signals (Fig. 2a, arrows). Additionally, these cell-free dots were only approx. one quarter as high as cells (not shown) as identified by a corresponding AFM scan (Fig. 2b, arrows). These findings indicate that these glycoconjugates were part of cell surfaces and remained on the glass after cell detachment (cell “footprints”).

Glycoconjugates of planktonic cells on filters In order to assess surface compounds of planktonic cells of *S. metallicus*^T grown on S^0 , 16 lectins were selected to stain cells settled on polycarbonate filters under fully hydrated conditions. The lectins BPA, Con A, GS-II, PMA, PNA, and SBA were detected to bind planktonic cells, as shown in Supplementary Fig. S1 and Table S1. Surface compounds were characterized as sugar monomers like mannose, glucose, galactose, N-acetylgalactosamine (GalNAc), and N-acetylglucosamine (GlcNAc). These sugars are generally found in cell wall structures of *Sulfolobales* (Albers and Meyer 2011).

Visualization of *S. metallicus*^T biofilm cells on S^0

Nucleic acid staining For staining of nucleic acids, the dyes SybrGreen, Syto 64, Syto 9, Syto 61, DDAO, and DAPI were used. Biofilms of *S. metallicus*^T on S^0 under fully hydrated conditions were visualized, as shown in Fig. 3. These were

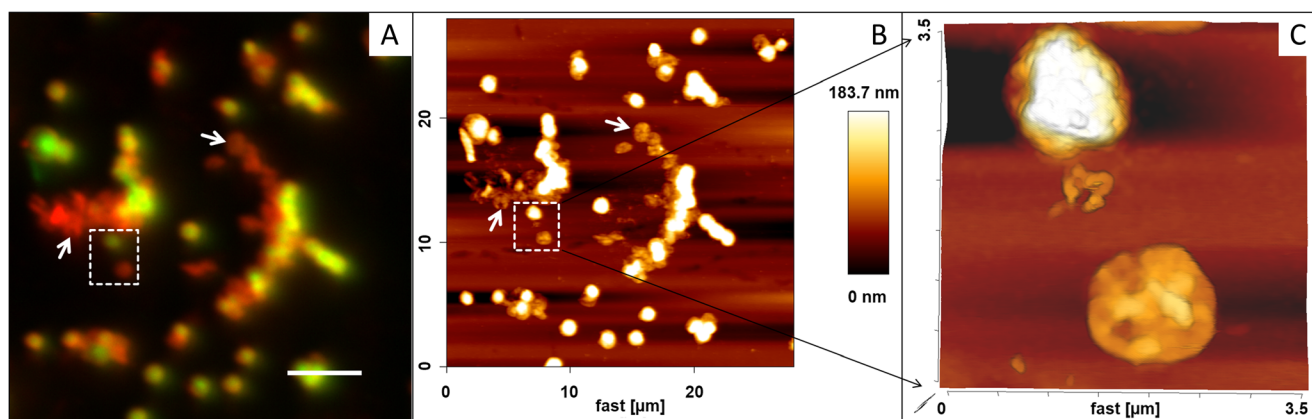


Fig. 2 Combined EFM with AFM Images of *S. metallicus*^T cells on glass slides. **a** (EFM) Cells stained by Syto 9 (green) and Con A-TRITC (red). **b** An AFM scanning in contact mode in air from the corresponding area in

a, **c** A 3-D image from an AFM scanning corresponding to the frame area in **a** and **b**. Size bar in **a** represents 5 μm

heterogeneous containing individual cells and large colonies after 5 days. Biofilm cells were often found in surface imperfections, while on flat areas, mostly, single cells were found. Apart from the cell distribution pattern, several extracellular DNA morphologies were visible. In Fig. 3b, cells were forming small colonies with approx. 10 μm. Diffuse DNA signals were covering individual cells. Thread-like and filamentous DNA was clearly visible (Fig. 3c, e, arrows). Some cells showed “cloud-like” signals and gave a blurred appearance, which was slightly bigger than normal cells (Fig. 3d). DAPI staining of biofilms showed also a cloud-like pattern, namely cells and materials (eDNA) connecting them (Fig. 3f). In case of *Acidianus* sp. DSMZ 29099, no such eDNA in biofilms was visible (Supplementary Fig. S2). Cell lysis caused by staining procedures was excluded because neutralization procedures did not result in cell disruption in our assays (not shown). However, an active excretion of DNA by cells due to a pH shock during staining cannot be ruled out.

Protein staining As shown in Fig. 4a–c, protein staining was revealed by several patterns: cell surfaces, areas near cell surfaces, and thread-like signals connecting cells. In comparison, these patterns of protein staining were not observed for biofilm cells of *Acidianus* sp. DSM 29099 (Fig. 4d). The presence of extracellular proteins in *S. metallicus*^T biofilms was coincident with the ATR-FTIR and conventional spectrophotometric analysis (Fig. 1 and Supplementary Table S2). Although it has been suggested that (thiol-rich) proteins are involved in attachment and sulfur activation, this is the first time that the presence of extracellular proteins has been verified by direct observation.

Amphiphilic compounds The dyes Nile red, FM1-63, and FM4-64 for lipophilic compounds were tested with biofilm cells of *S. metallicus*^T. FM1-43-stained cell surfaces and gave a “ring-like” (capsular) staining pattern (Fig. 4e). In contrast to protein or nucleic acid stains, no smear signals appeared. This

seems to indicate that lipophilic compounds, apart from cell surfaces, are not present on *S*⁰ surfaces, or their concentration is below the CLSM detection limit.

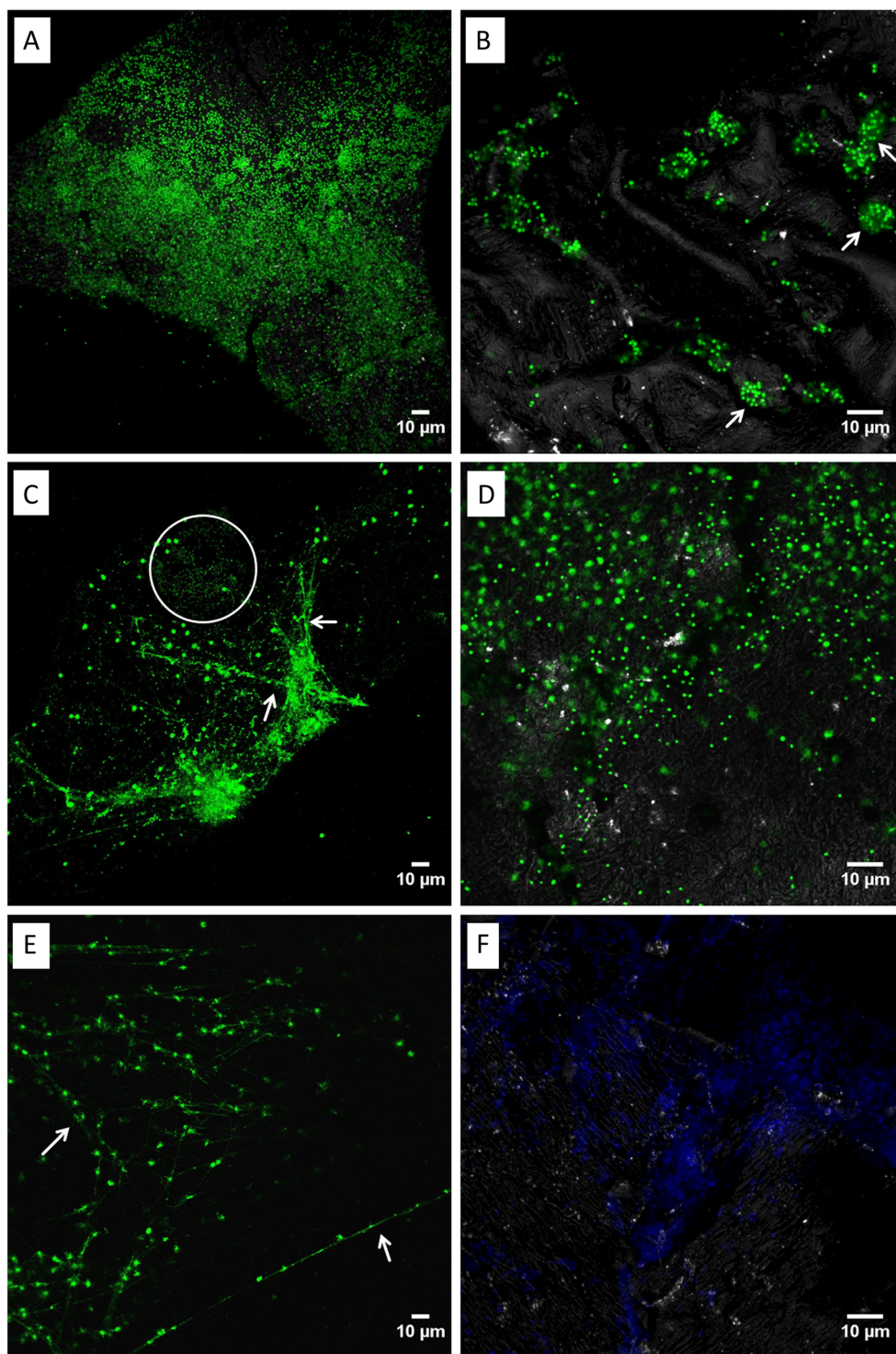
Visualization of glycoconjugates in biofilm cells

The screening of 72 commercially available lectins showed that 21 lectins bound to biofilm cells of *S. metallicus*^T (Table 2). When compared with the lectins reacting with EPS and cells of *Acidianus* sp. DSM 29099, only 8 of them recognized cell glycoconjugates of both archaeal species (Supplementary Table S3). The lectin AAL has been reported to react with acidophiles such as *F. acidiphilum*, *Acidianus*, and *S. metallicus* biofilms grown on pyrite. Also, it reacts with biofilms of *Acidianus* sp. DSM 29099 on *S*⁰ (Zhang et al. 2015). Interestingly, this lectin did not bind biofilm cells of *S. metallicus*^T on *S*⁰.

Binding patterns Among the positive lectins, two lectin-binding patterns became obvious. The first one represents lectin signals restricted to cell surfaces, named “capsular binding.” As shown in Fig. 5 and Table 2, 15 lectins showed this pattern. The second one corresponds to lectins, whose signals covered cell surfaces as well as extended areas close to the cells, named “colloidal binding.” In total, 6 lectins showed this pattern (Fig. 5 and Table 2). All positive lectins for both patterns are shown in Supplementary Figs. S3 and S4, respectively. These lectin-binding patterns were already reported for acidophilic archaeal biofilms on pyrite (Zhang et al. 2015).

Glycoconjugates on *S*⁰ Apart from the two types of lectin-binding patterns, various glycoconjugates were detected in biofilm cells of *S. metallicus*^T. These include glucose, galactose, mannose, fucose, sialic acids, GlcNAc, and GalNAc. Similar sugar moieties were reported to be present in biofilm cells of *Acidianus* sp. DSM 29099 grown on *S*⁰ (Zhang et al. 2015). In addition, we compared 16 selected lectins to stain

Fig. 3 Visualization of *S. metallicus*^T biofilms on S⁰ by nucleic acid stains. Maximum intensity projections of biofilms stained by SybrGreen (a–e) and DAPI (f). Diffuse (a, b, d) and thread (c, e, f) signals were visible. Cells were mostly detected on edges (b), holes (b), and cracks (f). Arrows indicate thread-like eDNA. Inside the circle in c, single cells were highlighted. Color allocation: green SybrGreen, blue DAPI. The sulfur surface is shown in reflection mode (grey)

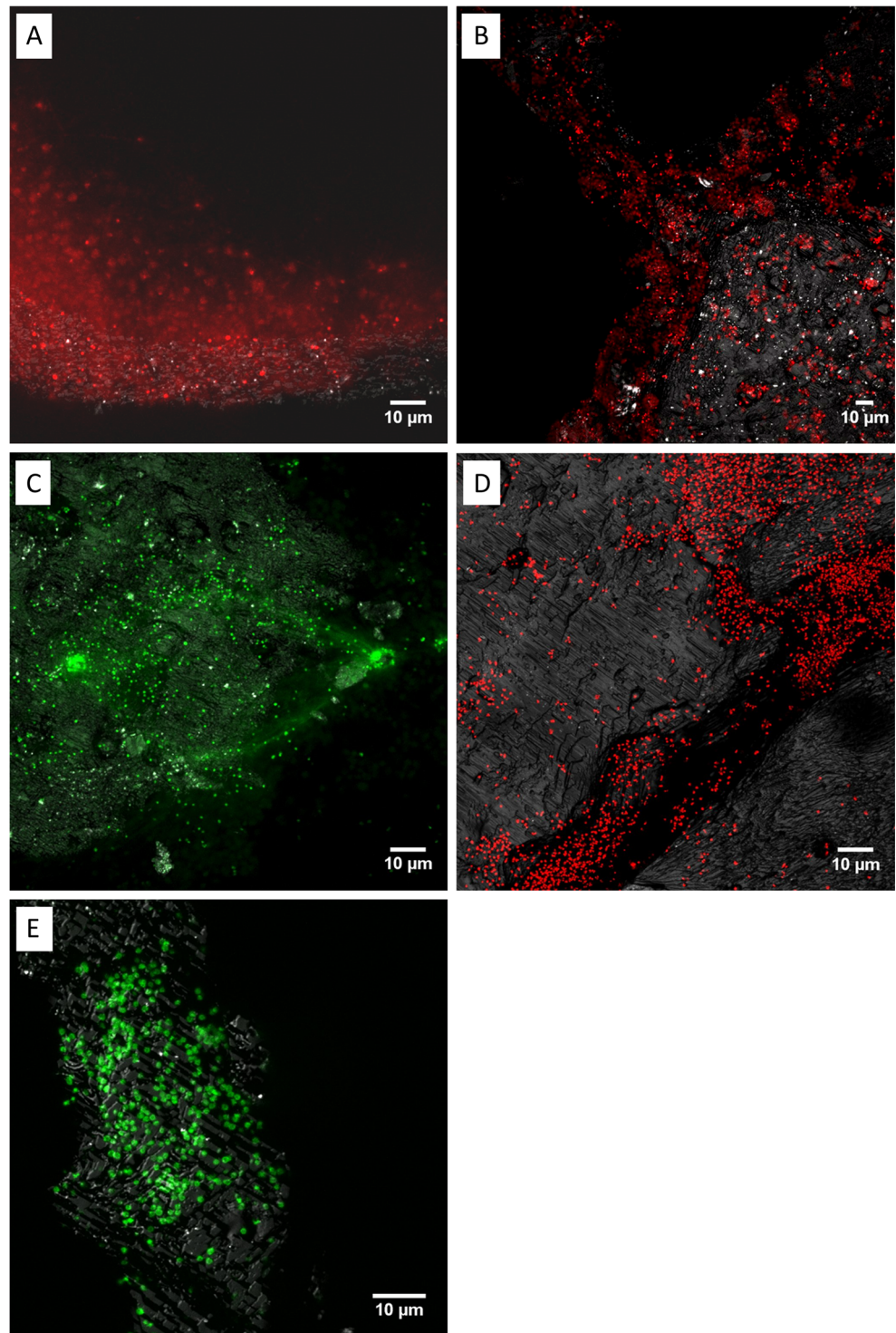


both, biofilm cells and planktonic cells of *S. metallicus*^T grown on S⁰. Among these, six lectins recognized biofilm cells and five bound to planktonic cells, respectively (Supplementary Table S1). Only Con A and PNA bound to both biofilm and planktonic cells. The lectin-binding results indicate that the cell surface polymers were quite similar, but not identical. Glucose, galactose, mannose, GlcNAc, and

GalNAc were detected on planktonic cell and biofilm cell surfaces. However, fucose was only present on biofilm cells.

AFM and EFM studies confirmed our CLSM observations of cell and EPS distribution of *S. metallicus*^T biofilms on S⁰. As shown in Fig. 6, biofilms in form of cell aggregates or microcolonies up to hundred micrometers in diameter were recorded by AFM scanning. Staining with Syto 9 and Con

Fig. 4 Visualization of thermophilic archaea biofilms on S^0 by protein and lipid stains. Maximum intensity projections of *S. metallicus*^T biofilms stained by SyproOrange (a–c) and FM1-43 (e). **d** Biofilms of *Acidianus* sp. DSM 29099 stained by SyproOrange. Color allocation: red SyproOrange (a, b, d), green SyproOrange (d) or FM1-43. The sulfur surface is shown in reflection mode (grey).



A-TRITC indicated the presence of EPS in biofilms. In addition, a heterogeneous distribution of biofilm cells and EPS was also observed.

Counter staining with a combination of nucleic acid-, protein-, lipophilic-, and glycoconjugate-specific fluorescent probes revealed localization and co-localization of these biomolecules. For instance, when SyproRed with

the FITC-conjugated lectins HHA or PMA were used to stain *S. metallicus*^T biofilms on sulfur, cells were shown to be embedded in an EPS matrix composed of extracellular proteins and glycoconjugates (Fig. 7 and Supplementary Fig. S5). When SyproOrange and DDAO were utilized, extracellular proteins and eDNA were simultaneously detected. A few cells were identified as

Table 2. Lectins binding to *S. metallicus*^T biofilm cells on S⁰

Lectin ^a	Source	Binding target	Binding pattern	Binding affinity
AAA	Eel serum (<i>Anguilla anguilla</i>)	Fuc	Capsular	+
CAA	<i>Caragana arborescens</i>	GalNAc	Capsular	+
Con A	Jack bean (<i>Canavalia ensiformis</i>)	Glc, Man	Capsular	+•
DBA	<i>Dolichos biflorus</i>	GalNAc	Capsular	+
ECA	<i>Erythrina cristagalli</i>	GalNAc, Gal	Capsular	+•
GNA	Snowdrop (<i>Galanthus nivalis</i>)	Man	Colloidal	+
HAA	Snail (<i>Helix aspersa</i>)	GalNAc	Capsular	+
HHA	<i>Amaryllis (Hippeastrum hybrid)</i>	Man	Colloidal	++
LAL	<i>Laburnum anagyroides</i>	Fuc	Colloidal	+•
LEA	Tomato (<i>Lycopersicon esculentum</i>)	GlcNAc	Colloidal	+
MAA	<i>Maackia amurensis</i>	Sia	Capsular	+•
MNA-G	<i>Morus nigra</i>	Gal	Capsular	+
NPA	<i>Narcissus pseudonarcissus</i>	Man	Colloidal	+•
PMA	<i>Polygonatum multiflorum</i>	Man	Colloidal	++•
PNA	Peanut (<i>Arachis hypogea</i>)	Gal	Capsular	+•
PTA	<i>Psophocarpus tetragonolobus</i>	GalNAc	Capsular	+
RPA	Black locust (<i>Robinia pseudacacia</i>)	GalNAc	Capsular	+
TKA	<i>Trichosanthes kirilowii</i>	Gal	Capsular	+
UEA-I	Furze gorse (<i>Ulex europaeus</i>)	Fuc	Capsular	+
VGA	<i>Vicia graminea</i>	GlcNAc	Capsular	+
VVA	<i>Vicia villosa</i>	GalNAc	Capsular	+•

Examination of no less than three different sulfur prills for deciding positive or negative lectin staining. Only positive ones are listed in the table. Biological replicates were re-checked for the data reproducible. More than 100 images were recorded in our data library (UFZ, Magdeburg) to elucidate the interesting findings during microscopic observations. Visual observation of the binding affinity was recorded according to Staudt et al. 2003.

Glu glucose, *Man* mannose, *Fuc* fucose, *Gal* galactose, *Sia* sialic acid, *GalNAc* N-acetylgalactosamine, *GlcNAc* N-acetylglucosamine; + fair, +• good, ++ very good, ++• extremely good

^a For details of the lectins, see Zhang et al. 2015.

“dead,” as indicated by DDAO staining (Fig. 8). Nevertheless, in some cases, the combination of different dyes did not work properly. For example, when DAPI was combined with the lectin HHA-FITC, lectin signals were fuzzy rather than showing clear patterns (not shown). The reasons for the “fuzzy signals” are unclear. In addition, sulfur surfaces have a strong reflection of red light, which interfered with the use of TRITC-conjugated lectins. Unfortunately, under these conditions, the separation of the red signal from TRITC from the surface reflection was not possible.

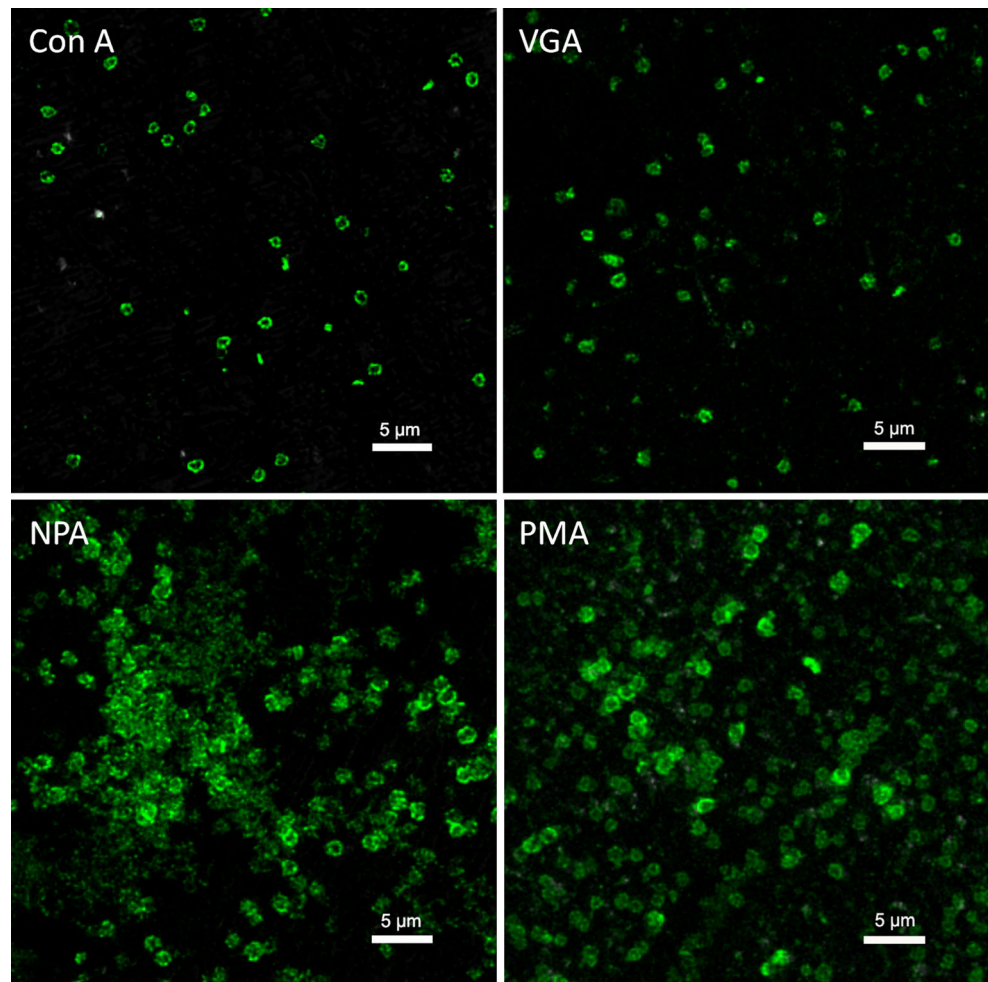
The biofilm matrix of *S. metallicus*^T on S⁰ is flexible

During CLSM observations, biofilm cells were often observed to be loosely attached or immobile on sulfur surfaces. Major parts of the biofilms were slightly vibrating (Supplementary Movie S1). A few cells were either swimming away or moving back and forth. Interestingly, some cells seem to be either fixed on the surface by stalks or embedded in a gel matrix, in which

cells may be held by loose polymers (Figs. 7 and 8 and Supplementary Fig. S5), or connected by thread-like nucleic acid compounds (Fig. 3). A lateral movement of cells of *Sulfolobus* on sulfur surfaces has been observed, but attempts to directly visualize the “stalks” or connecting materials were unsuccessful (Weiss 1973). For *Sulfolobus* this is its first direct observation that biofilm cells are embedded in flexible EPS matrix. EPS networks or thread-like structures mediating cell-sulfur interaction are possibly in a nanoscale-range. Currently, no technique is available to visualize them routinely in situ. Summarizing, (1) biofilm cells are embedded in a gel-like matrix, (2) some cells are mobile either self-propelled by cellular appendages, e.g., archaella (Jarrell and Albers 2012) or by “Brownian motion,” and (3) these biofilm matrixes are heterogeneous, complex mixtures, and only partly stainable by dyes.

The negative result of Calcoflour White M2R (not shown) staining indicates the absence of β -polysaccharides like cellulose in the biofilm matrix of *S. metallicus*^T on S⁰.

Fig. 5 Lectins showing “capsular” and “colloidal” binding patterns to *S. metallicus*^T biofilms. Maximum intensity projections with deconvolution process of *S. metallicus*^T biofilms on elemental sulfur stained by lectins Con A, VGA, NPA, and PMA are shown. Signals of Con A and VGA were mostly restricted to cell boundaries and showed a “capsular binding” pattern. Signals of NPA and PMA were found on cell surfaces and also on sulfur surfaces apart from cells. Color allocation: *green* FITC-conjugated lectins. For all positive lectin-binding results, see Supplementary Figs. S3 and S4



Discussion

Few studies have shown biofilms of thermophilic archaea. Biofilms with “carpet-like” structures by *Sulfolobus*

solfatarius and *Sulfolobus tokodaii* and high density tower-like structures by *Sulfolobus acidocaldarius* were reported (Koerdet et al. 2010). Three type IV pili-like cell appendages of *S. acidocaldarius* were found to be involved in cell

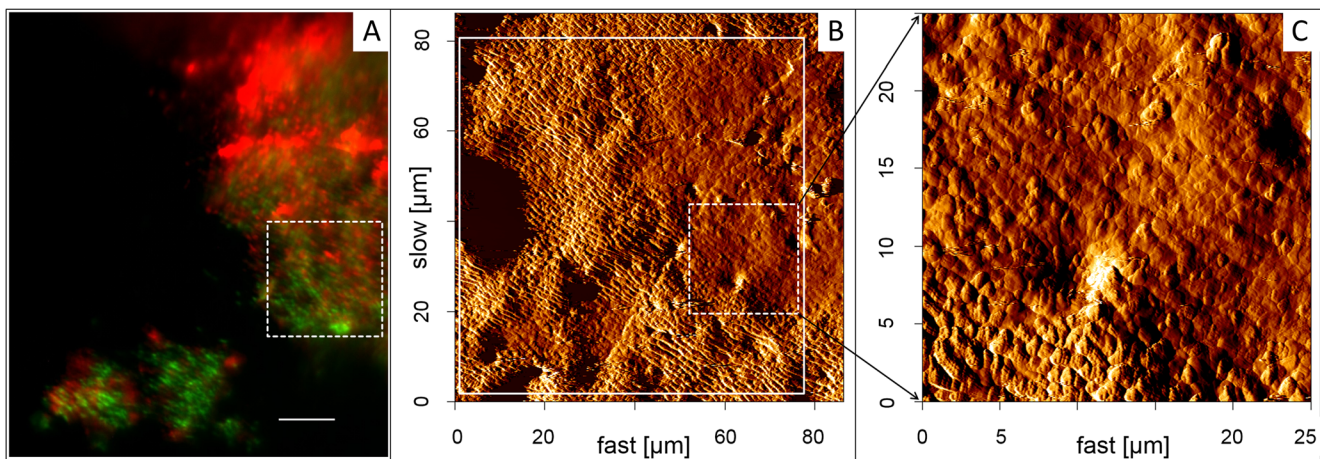


Fig. 6 Images of biofilm cells of *S. metallicus*^T on S⁰ by EFM (a) combined with AFM (b, c). a Cells stained by Syto 9 (green) and TRITC-Con A (red). b An AFM scanning (solid frame) in contact mode in air corresponding to the area in a. c Details from an AFM scanning

corresponding to the frame (dashed line) area in a and b. Arrows in c indicate visible individual cells inside biofilms on elemental sulfur. Bar in a represents 10 μm

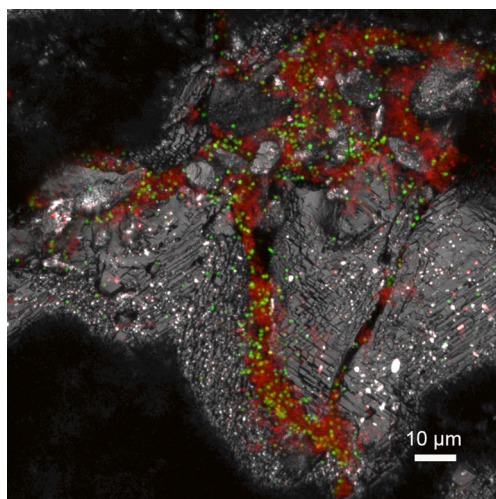


Fig. 7 Maximum intensity projections of *S. metallicus*^T biofilms on S⁰ stained by SyproRed and subsequently by lectin HHA-FITC. Take notice of lectin signal at the cell surface and protein signal indicating extended EPS around the cell colonies. Cells are held together by means of EPS matrix. Color allocation: *green* HHA-FITC, *red* SyproRed, *grey* reflection

colonization and biofilm formation on glass surfaces (Henche et al. 2012). Cell appendages like pili or flagella were shown to be essential for initial attachment to various surfaces (e.g., glass, mica, pyrite, and carbon-coated gold grids) of *S. solfataricus* (Zolghadr et al. 2010). The enzymes mannosidase and galactosidase in *S. solfataricus* were first described as playing a role in archaeal EPS formation (Koerdts et al. 2012). However, these studies were carried out with cells grown in complex media and, almost always, biofilms were developed on non-natural substratum surfaces (e.g., glass slides). Consequently, there is a very limited knowledge of biofilm formation and EPS production by *Sulfolobus* species

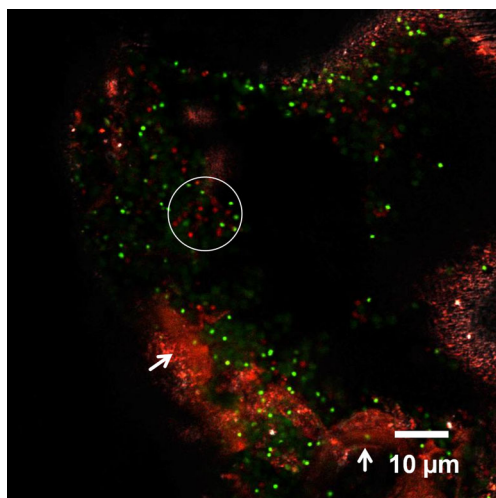


Fig. 8 Maximum intensity projections of *S. metallicus*^T biofilms on S⁰ stained by SyproOrange and subsequently by DDAO. Inside the *circle*, several red cells with DDAO signals are *highlighted*. *Arrows* indicate polymers stained both by SyproOrange and DDAO. Color allocation: *green* SyproOrange, *red* DDAO, *grey* reflection

grown on solid inorganic substrates (S⁰ or pyrite). In the present study, we applied FTIR, various stains, and CLSM to examine biofilms of *S. metallicus* 6482^T grown on S⁰ (one of their natural substrates) in order to get more details of archaeal EPS characteristics and their involvement in interactions with S⁰.

The combination of AFM and EFM allows to understand both biological origins and their detailed structures at a high resolution (Harneit et al. 2006; Mangold et al. 2008; Zhang et al. 2014). Such a combination enabled us to detect the footprints of *S. metallicus*^T after detachment (Fig. 2). These microbial footprints have been reported to occur in *A. ferrooxidans* or *S. thermosulfidooxidans* grown on pyrite (Mangold et al. 2008; Becker et al. 2011) and in a mixed culture of mesophilic acidophilic chemolithotrophs grown on sphalerite, where *Leptospirillum ferriphilum* was predominant (Ghorbani et al. 2012). For thermoacidophilic archaea, this is the first observation of such phenomenon on rigid surfaces. Clearly, sugar residues like mannose and glucose were involved in cellular attachment to surfaces. Further analysis showed that these two sugars accounted for 90 % of total carbohydrates in *S. metallicus*^T EPS, both from capsular and colloidal fractions (R. Zhang and V. Blanchard, unpublished). Nevertheless, to understand the initial interaction of *S. metallicus*^T with surfaces, the nature of these footprints needs to be further analyzed.

Extracellular DNA was first described for *Pseudomonas aeruginosa* biofilms (Whitchurch et al. 2002) and is thought to be a critical component of the biofilm matrix (Dominiak et al. 2011; Okshevsky and Meyer 2013). Biofilm eDNA originates either from cell lysis or from an (unknown) excretion process (Flemming and Wingender 2010). In the present study, the nucleic acid staining indicates the existence of eDNA with different morphologies on the S⁰ surfaces after biofilm formation (Fig. 3). The presence of eDNA in EPS from biofilms was also confirmed by ATR-FTIR (Fig. 2) and colorimetric determination (Supplementary Table S2). However, no eDNA in capsular EPS or colloidal EPS was found. In addition, our previous study showed that no eDNA was detected in *S. metallicus*^T biofilms on pyrite (Zhang et al. 2015). Thus, it is reasonable to assume that eDNA excretion by *S. metallicus*^T is substrate-mediated. The presence of eDNA in *S. metallicus*^T biofilms on S⁰ may be essential to convey certain advantages for biofilm integrity, stability, and cell survival.

Protein secretion has been proved in *S. solfataricus*, *S. acidocaldarius*, and *S. tokodaii* grown on medium supplemented with glucose, casamino acids, starch, and/or NZ-amine as a limited process. Only a few proteins were detected in the bulk solution (Ellen et al. 2010). Our present study showed similar results. Mainly carbohydrates and few proteins were present in the colloidal EPS fraction of *S. metallicus*^T grown on S⁰ (Supplementary Table S2). However, proteins were dominating the EPS from biofilms on S⁰.

The production of proteins in biofilms on sulfur surfaces suggests that these proteins may have a structural role in stabilizing biofilm structures as well as a functional role in the activation of S^0 and transportation of linear polysulfides for their subsequent oxidation. A high-throughput proteomic study of *A. ferrooxidans* revealed that several proteins were related to biofilm formation on pyrite (Vera et al., 2013a). Future omics projects of *S. metallicus*^T would facilitate analysis and understanding of the role of extracellular proteins in sulfur colonization and metabolism.

Previous reports claimed that lipids/phospholipids play important roles in microbial attachment and the dissolution of S^0 (Beebe and Umbreit 1971; Umbreit et al. 1942). In the present study, lipids were visualized by CLSM combined with specific stains. However, these were cell surface-associated. Probably in case of *S. metallicus*^T, lipophilic compounds play a role in initial attachment by interacting with the hydrophobic S^0 surface. However, in the later stages of cell- S^0 interaction and dissolution, proteins rather than lipids seem to be the major functional components of EPS.

Generally, initial attachment, irreversible attachment, mature biofilm, and detachment are the four major steps/periods of a biofilm cycle (Stoodley et al. 2002). After initial attachment, EPS are excreted by cells in order to enlarge spaces for metabolic activities. We detected two lectin-binding patterns of *S. metallicus*^T biofilms on S^0 : “capsular” and “colloidal.” The former represents glycoconjugates tightly associated with cell surface. The later indicates EPS glycoconjugates which were not only present on cell surface but also spread on S^0 surface at which it was cell free. These colloidal EPS actively excreted by cells might be also involved in modification of S^0 surfaces (from hydrophobic to hydrophilic) and S^0 activation. Our results also support the theory that cells excrete EPS in order to extend reacting spaces, which has been postulated in the case of microbial dissolution of metal sulfides, e.g., pyrite (Sand et al. 1998; Vera et al. 2013b).

It is well known that biofilm cells are phenotypically distinct from their planktonic counterparts (Vera et al. 2013a). Among three *Sulfolobus* spp., planktonic and biofilm lifestyles have distinctive influence on the physiology of cells (Koerdt et al. 2011). In this context, biofilm and planktonic cells of *S. metallicus*^T can be distinguished by using certain lectins. Lectins have also revealed differences in the EPS composition of *T. thioparus* biofilms developed under alternative growth modes (Boretska et al. 2013).

Due to the huge structural diversity of EPS matrix, especially polysaccharides, there is neither a general stain for EPS compounds nor a fluorescent stain for all types of polysaccharides. FLBA involves the tests of a specific biofilm against a range of lectins (Neu et al. 2001). The selected 21 positive lectins (Table 2) enabled us to simultaneously visualize and characterize some glycoconjugates and additional EPS compounds when combined with other stains. In addition, these

selected lectins may be useful to distinguish *S. metallicus*^T in mixed biofilm populations.

It has been shown that extracellular proteins of cells of *Sulfolobus* are highly glycosylated. The high glycosylation density in the S-layer represents an adaptation to the high temperature of their acidic environment (Jarrell et al. 2014; Meyer and Albers 2013). The overlapping of protein and lectin signals suggests that some lectins may also bind to some glycoproteins present in S-layers of biofilms of *S. metallicus*^T (Fig. 7) (Zhang et al. 2015).

Four acid-stable fluorescent dyes were reported for visualizing acidophilic microorganisms in acid mine drainage communities (Brockmann et al. 2010). However, these stains are in general for cell staining and some binding properties are not fully clear. Acid-stable lectins/stains reacting with compounds of acidophilic leaching microorganisms will be necessary for an improved analysis of microbial biofilms in bioleaching process. In this context, isolation of lectins from acidophiles seems to be meaningful.

In summary, CLSM combined with various fluorophores was used to map the distribution of macromolecules of EPS and differentiate several compounds like polysaccharides, proteins, lipids, and nucleic acids of *S. metallicus*^T biofilm cells and the developing EPS matrix. Polysaccharides, proteins, and eDNA were found in biofilm matrix. Twenty-one lectins were found to be useful for visualization and monitoring *S. metallicus* biofilms. Different lectin reacting patterns including capsular and colloidal binding patterns were detected. Lectin-specific EPS glycoconjugates indicated that fucose, mannose, glucose, galactose, GlcNAc, and GalNAc were present on S^0 -grown cells. The detection of eDNA and extracellular proteins in biofilm EPS of *S. metallicus* suggests their potential roles in biofilm formation and stabilization of biofilm structures. Our data improve the understanding of acidophilic archaeal biofilm organization and interactions with S^0 .

Acknowledgments We thank Dr. Supratim Banerjee (Institute of Organic Chemistry, Universität Duisburg-Essen) for the help of FTIR measurements. R. Z. acknowledges China Scholarship Council (CSC) for financial support (no. 2010637124).

Conflict of interest The authors declare that they have no competing interests.

References

- Albers S-V, Meyer BH (2011) The archaeal cell envelope. *Nat Rev Microbiol* 9:414–426
- Arredondo R, Garcia A, Jerez CA (1994) Partial removal of lipopolysaccharide from *Thiobacillus ferrooxidans* affects its adhesion to solids. *Appl Environ Microbiol* 60:2846–2851
- Becker T, Gorham N, Shiers D, Watling H (2011) In situ imaging of *Sulfobacillus thermosulfidooxidans* on pyrite under conditions of variable pH using tapping mode atomic force microscopy. *Process Biochem* 46:966–976

- Beebe JL, Umbreit W (1971) Extracellular lipid of *Thiobacillus thiooxidans*. J Bacteriol 108:612–614
- Bellenberg S, Leon-Morales C-F, Sand W, Vera M (2012) Visualization of capsular polysaccharide induction in *Acidithiobacillus ferrooxidans*. Hydrometallurgy 129:82–89
- Blais J-F, Tyagi R, Meunier N, Auclair J (1994) The production of extracellular appendages during bacterial colonization of elemental sulphur. Process Biochem 29:475–482
- Boretska M, Bellenberg S, Moshynets O, Pokholenko I, Sand W (2013) Change of extracellular polymeric substances composition of *Thiobacillus thiooparus* in presence of sulfur and steel. J Microb Biochem Technol 5:68–73
- Bradford MM (1976) A rapid and sensitive method for the quantitation of microgram quantities of protein utilizing the principle of protein-dye binding. Anal Biochem 72:248–254
- Brockmann S, Arnold T, Schweder B, Bernhard G (2010) Visualizing acidophilic microorganisms in biofilm communities using acid stable fluorescence dyes. J Fluoresc 20:943–951
- Bryant R, Costerton J, Laishley E (1984) The role of *Thiobacillus albertis* glycocalyx in the adhesion of cells to elemental sulfur. Can J Microbiol 30:81–90
- Burton K (1956) A study of the conditions and mechanism of the diphenylamine reaction for the colorimetric estimation of deoxyribonucleic acid. Biochem J 62:315–323
- Castro L, Zhang R, Muñoz JA, González F, Blázquez ML, Sand W, Ballester A (2014) Characterization of exopolymeric substances (EPS) produced by *Aeromonas hydrophila* under reducing conditions. Biofouling 30:501–511
- Dominiak DM, Nielsen JL, Nielsen PH (2011) Extracellular DNA is abundant and important for microcolony strength in mixed microbial biofilms. Environ Microbiol 13:710–721
- Dopson M, Johnson DB (2012) Biodiversity, metabolism and applications of acidophilic sulfur-metabolizing microorganisms. Environ Microbiol 14:2620–2631
- Dubois M, Gilles KA, Hamilton JK, Rebers P, Smith F (1956) Colorimetric method for determination of sugars and related substances. Anal Chem 28:350–356
- Dutrizac J (1990) Elemental sulphur formation during the ferric chloride leaching of chalcopyrite. Hydrometallurgy 23:153–176
- Ellen AF, Albers S-V, Driessen AJ (2010) Comparative study of the extracellular proteome of *Sulfolobus* species reveals limited secretion. Extremophiles 14:87–98
- Flemming H-C, Wingender J (2010) The biofilm matrix. Nat Rev Microbiol 8:623–633
- Flemming H-C, Neu TR, Wozniak DJ (2007) The EPS matrix: the “house of biofilm cells”. J Bacteriol 189:7945–7947
- Fröls S (2013) Archaeal biofilms: widespread and complex. Biochem Soc Trans 41:393–398
- Ghorbani Y, Petersen J, Harrison ST, Tupikina OV, Becker M, Mainza AN, Franzidis J-P (2012) An experimental study of the long-term bioleaching of large sphalerite ore particles in a circulating fluid fixed-bed reactor. Hydrometallurgy 129:161–171
- Harneit K, Göksel A, Kock D, Klock J-H, Gehrke T, Sand W (2006) Adhesion to metal sulfide surfaces by cells of *Acidithiobacillus ferrooxidans*, *Acidithiobacillus thiooxidans* and *Leptospirillum ferrooxidans*. Hydrometallurgy 83:245–254
- Henche AL, Koerdt A, Ghosh A, Albers SV (2012) Influence of cell surface structures on crenarchaeal biofilm formation using a thermostable green fluorescent protein. Environ Microbiol 14:779–793
- Jarrell KF, Albers S-V (2012) The archaeum: an old motility structure with a new name. Trends Microbiol 20:307–312
- Jarrell KF, Ding Y, Meyer BH, Albers S-V, Kaminski L, Eichler J (2014) N-linked glycosylation in Archaea: a structural, functional, and genetic analysis. Microbiol Mol Biol Rev 78:304–341
- Kletzin A (2008) Oxidation of sulfur and inorganic sulfur compounds in *Acidianus ambivalens*. In: Dahl C, Friedrich CG (Eds) Microbial sulfur metabolism. Springer, Heidelberg, pp 184–201
- Knickerbocker C, Nordstrom D, Southam G (2000) The role of “blebbing” in overcoming the hydrophobic barrier during biooxidation of elemental sulfur by *Thiobacillus thiooxidans*. Chem Geol 169:425–433
- Koerdt A, Gödeke J, Berger J, Thormann KM, Albers S-V (2010) Crenarchaeal biofilm formation under extreme conditions. PLoS One 5:e14104
- Koerdt A, Orell A, Pham TK, Mukherjee J, Wlodkowski A, Karunakaran E, Biggs CA, Wright PC, Albers S-V (2011) Macromolecular fingerprinting of *Sulfolobus* species in biofilm: a transcriptomic and proteomic approach combined with spectroscopic analysis. J Proteome Res 10:4105–4119
- Koerdt A, Jachlewski S, Ghosh A, Wingender J, Siebers B, Albers S-V (2012) Complementation of *Sulfolobus solfataricus* PBL2025 with an α -mannosidase: effects on surface attachment and biofilm formation. Extremophiles 16:115–125
- Little B, Ray R, Pope R (2000) Relationship between corrosion and the biological sulfur cycle: a review. Corrosion 56:433–443
- Liu H-C, Xia J-L, Nie Z-Y, Peng A-A, Ma C-Y, Zheng L, Zhao Y-D (2013) Comparative study of sulfur utilization and speciation transformation of two elemental sulfur species by thermoacidophilic Archaea *Acidianus manzaensis* YN-25. Process Biochem 48:1855–1860
- Mackintosh ME (1978) Nitrogen fixation by *Thiobacillus ferrooxidans*. J Gen Microbiol 105:215–218
- Mangold S, Harneit K, Rohwerder T, Claus G, Sand W (2008) Novel combination of atomic force microscopy and epifluorescence microscopy for visualization of leaching bacteria on pyrite. Appl Environ Microbiol 74:410–415
- Meyer BH, Albers S-V (2013) Hot and sweet: protein glycosylation in Crenarchaeota. Biochem Soc Trans 41:384–392
- Naumann D, Helm D, Labischinski H (1991) Microbiological characterizations by FT-IR spectroscopy. Nature 351:81–82
- Neu TR, Swerhone GD, Lawrence JR (2001) Assessment of lectin-binding analysis for in situ detection of glycoconjugates in biofilm systems. Microbiology 147:299–313
- Ng F-W, Dawes E (1973) Chemostat studies on the regulation of glucose metabolism in *Pseudomonas aeruginosa* by citrate. Biochem J 132:129–140
- Nichols PD, Michael Henson J, Guckert JB, Nivens DE, White DC (1985) Fourier transform-infrared spectroscopic methods for microbial ecology: analysis of bacteria, bacteri-polymer mixtures and biofilms. J Microbiol Methods 4:79–94
- Nie Z-Y, Liu H-C, Xia J-L, Zhu H-R, Ma C-Y, Zheng L, Zhao Y-D, Qiu G-Z (2014) Differential utilization and transformation of sulfur allotropes, μ -S and α -S₈, by moderate thermoacidophile *Sulfolobus thermosulfidooxidans*. Res Microbiol 165:639–646
- Okshevsky M, Meyer RL (2013) The role of extracellular DNA in the establishment, maintenance and perpetuation of bacterial biofilms. Crit Rev Microbiol 1-11
- Orell A, Fröls S, Albers S-V (2013) Archaeal biofilms: the great unexplored. Annu Rev Microbiol 67:337–354
- Parikh SJ, Chorover J (2006) ATR-FTIR spectroscopy reveals bond formation during bacterial adhesion to iron oxide. Langmuir 22:8492–8500
- Peng AA, Xia JL, Liu HC, Zhu W, Zhang RY, Zhang CG, Nie ZY (2013) Thiol-rich proteins play important role in adhesion and sulfur oxidation process of *Acidithiobacillus ferrooxidans*. Adv Mater Res 825:137–140
- Rodríguez Y, Ballester A, Blázquez M, Gonzalez F, Muñoz J (2003) New information on the chalcopyrite bioleaching mechanism at low and high temperature. Hydrometallurgy 71:47–56

- Rohwerder T, Sand W (2003) The sulfane sulfur of persulfides is the actual substrate of the sulfur-oxidizing enzymes from *Acidithiobacillus* and *Acidiphilium* spp. *Microbiology* 149:1699–1710
- Rohwerder T, Sand W (2007) Oxidation of inorganic sulfur compounds in acidophilic prokaryotes. *Eng Life Sci* 7:301–309
- Sand W (1985) The influence of four detergents on the substrate oxidation by *Thiobacillus ferrooxidans*. *Environ Technol* 6:439–444
- Sand W, Gehrke T, Hallmann R, Schippers A (1998) Towards a novel bioleaching mechanism. *Miner Process Extr Metall Rev* 19:97–106
- Schmitt J, Flemming H-C (1998) FTIR-spectroscopy in microbial and material analysis. *Int Biodeterior Biodegrad* 41:1–11
- Staudt C, Horn H, Hempel D, Neu T (2003) Screening of lectins for staining lectin-specific glycoconjugates in the EPS of biofilms. In: Lens P, O'Flaherty V, Moran AP, Stoodley P, Mahony T (eds) *Biofilms in medicine, industry and environmental technology*. IWA Publishing, London, pp 308–327
- Stoodley P, Sauer K, Davies D, Costerton JW (2002) Biofilms as complex differentiated communities. *Annu Rev Microbiol* 56: 187–209
- Suci P, Siedlecki K, Palmer R, White D, Geesey G (1997) Combined light microscopy and attenuated total reflection fourier transform infrared spectroscopy for integration of biofilm structure, distribution, and chemistry at solid-liquid interfaces. *Appl Environ Microbiol* 63: 4600–4603
- Takeuchi TL, Suzuki I (1997) Cell hydrophobicity and sulfur adhesion of *Thiobacillus thiooxidans*. *Appl Environ Microbiol* 63:2058–2061
- Umbreit W, Vogel H, Vogler K (1942) The significance of fat in sulfur oxidation by *Thiobacillus thiooxidans*. *J Bacteriol* 43:141–148
- Vera M, Krok B, Bellenberg S, Sand W, Poetsch A (2013a) Shotgun proteomics study of early biofilm formation process of *Acidithiobacillus ferrooxidans* ATCC 23270 on pyrite. *Proteomics* 13:1133–1144
- Vera M, Schippers A, Sand W (2013b) Progress in bioleaching: fundamentals and mechanisms of bacterial metal sulfide oxidation—part A. *Appl Microbiol Biotechnol* 97:7529–7541
- Weiss R (1973) Attachment of bacteria to sulphur in extreme environments. *J Gen Microbiol* 77:501–507
- Whitchurch CB, Tolker-Nielsen T, Ragas PC, Mattick JS (2002) Extracellular DNA required for bacterial biofilm formation. *Science* 295:1487–1487
- Zhang C-G, Xia J-L, Zhang R-Y, Peng A-A, Nie Z-Y, Qiu G-Z (2008a) Comparative study on effects of Tween-80 and sodium isobutylxanthate on growth and sulfur-oxidizing activities of *Acidithiobacillus albertensis* BY-05. *T Nonferr Metal Soc* 18: 1003–1007
- Zhang C-G, Zhang R-Y, Xia J-L, Zhang Q, Z-Y NIE (2008b) Sulfur activation-related extracellular proteins of *Acidithiobacillus ferrooxidans*. *T Nonferr Metal Soc* 18:1398–1402
- Zhang R, Bellenberg S, Castro L, Neu TR, Sand W, Vera M (2014) Colonization and biofilm formation of the extremely acidophilic archaeon *Ferroplasma acidiphilum*. *Hydrometallurgy* 150:245–252
- Zhang RY, Neu TR, Bellenberg S, Kuhlicke U, Sand W, Vera M (2015) Use of lectins to in situ visualize glycoconjugates of extracellular polymeric substances in acidophilic archaeal biofilms. *Microb Biotechnol* 8:448–461
- Zippel B, Neu T (2011) Characterization of glycoconjugates of extracellular polymeric substances in tufa-associated biofilms by using fluorescence lectin-binding analysis. *Appl Environ Microbiol* 77:505–516
- Zolghadr B, Klingl A, Koerdt A, Driessen AJ, Rachel R, Albers S-V (2010) Appendage-mediated surface adherence of *Sulfolobus solfataricus*. *J Bacteriol* 192:104–110